Radio-frequency-assisted electromagnetically induced transparency

Carl Basler, Jonas Grzesiak, and Hanspeter Helm
Department of Molecular and Optical Physics, Freiburg University, Stefan-Meier-Strasse 19, 79104 Freiburg, Germany
(Received 12 May 2015; published 7 July 2015)

A near-resonant rf field pumping the hyperfine transition between the two ground states of a Λ-shaped dark resonance leads to a resonance tripling, each component displaying electromagnetically induced transparency (EIT). We investigate the three resonances under high spectral and temporal resolution. The triplet formation is analogous to that of the Mollow triplet but distinct in that the role played by the spontaneous emission rate is now taken by the one-photon scattering rate of the optical Raman transition. Complex phase relations exist between the three em fields under EIT conditions. We explain our observations using numerical solutions of the quantum master equation as well as a simple analytical dressed-state model.

DOI: 10.1103/PhysRevA.92.013809 PACS number(s): 42.50.Gy, 32.80.Qk, 32.30.−r

I. INTRODUCTION

Radio-frequency control of electromagnetically induced transparency (EIT) [1] is envisioned in several quantum optics applications ranging from creating artificial selection rules for frequency-selective quantum operations [2–5], to controlled anticrossings by symmetry breaking in circuit quantum electrodynamics [6], to rf-driven EIT for generation of phase gratings for optical switching [7–9]. Theory has predicted new narrow resonances, limited in width only by the ground-state decoherence, with the prospect of engineering both the position and width of the narrow resonances by rf amplitude, frequency and phase, thus promising intimate control over dispersion and group velocity [2,10–12].

Radio-frequency control is, for example, accomplished by rf fields whose frequency is near resonant with the difference frequency of the optical fields which establish a Raman connection in a Λ system between two ground states. In resonant Raman interaction of two hyperfine states $|1\rangle$ and $|2\rangle$, atoms are optically pumped into a so-called dark state [1], which is transparent (dark) to the optical fields that connect the two states to a common excited level $|3\rangle$. For long interaction times, the ground states form the dark nonstationary superposition

$$|\psi_D(z,t)\rangle = \frac{1}{\sqrt{2}}(|1\rangle - e^{i(\omega_{hf}t+kz-\phi)}|2\rangle). \quad (1)$$

Here we assume, for simplicity, equal Rabi frequencies $g_1 = g_2 = g$ of the two optical fields with wave-vector difference $k = k_2 - k_1$ and phase difference $\phi = \phi_2 - \phi_1$. State $|2\rangle$ lies higher in energy by ω_{hf}, the hyperfine splitting.

The presence of a radio-frequency field which connects $|1\rangle$ and $|2\rangle$ in a magnetic dipole transition can modify condition (1), as shown in the rf pulse-area dependence of the Ramsey fringe patterns reported by Shahriar *et al.* [13]. Li *et al.* [14] demonstrated that the optical fields establish a spatial pattern of the relative phase kz of the dark state which can be constructive or destructive to rf excitation. Wilson *et al.* [15] studied spin transitions of the nitrogen-vacancy center in diamond and observed tripling of the EIT resonance when the rf frequency ω_{rf} matched the hyperfine splitting. In the experiments [13,14], rf signals at frequency ω_{rf} were employed and were also used to generate the optical frequency difference $\Delta\omega_L = \omega_{L1} - \omega_{L2}$. As a consequence, the three-photon resonance condition was automatically enforced.

In the work presented here we use two independent optical fields which are phase locked with respect to each other. A separate tunable and phase-shiftable rf signal is used which is phase referenced to the laser frequency difference. This allows us to study the interplay between the detunings $\Delta\omega_L, \phi$, and ϕ_{rf} and the rf detuning from resonance, $\delta_{rf} = \omega_{hf} - \omega_{rf}$, in stationary and time-dependent fashion. We show that the full spectrum includes nonlinear resonances, analogous to the sidebands in the Mollow triplet [16], and explain the sidebands with a dressed state model for the rf coupled dark state. We also confirm the predicted resonance narrowing [10].

II. THEORY

Among the many EIT resonances which can be constructed in rubidium, three belonging to the lowest energy D_1 transition in ^{87}Rb are degenerate in first-order at low magnetic field. Under high resolution they separate into the R^0, R^+, and R^- dark resonance spectrum of Fig. 1.

At low laser intensity and small dephasing rate the three resonances are spectrally well separated. The optical two-photon detuning δ measures the detuning of the optical frequency difference and the hyperfine splitting $\delta = \Delta\omega_L - \omega_{hf}$.

The R^0 resonance involves two Zeeman levels in the ground state and two Zeeman levels in the excited state. To simplify the description we neglect the small Zeeman splitting in the excited state and treat the R^0 resonance as a three-level system, the two ground states at energies ω_1 and ω_2 and one excited state at ω_3. To simplify notation we absorb the small quadratic Zeeman level shift (2 kHz at 3 G) into the hyperfine splitting ω_{hf}. In order to describe the absorption of lasers 1 and 2 in the presence of the rf field we introduce levels dressed by rf photons with N counting the number of rf photons as shown in Fig. 2.

In a frame rotating with the frequencies of the fields we write for the state vector

$$|\tilde{\Psi}\rangle = \tilde{\psi}_{2,N-1}|2,N-1\rangle + \tilde{\psi}_{1,N}|1,N\rangle + \tilde{\psi}_{2,N}|2,N\rangle + \tilde{\psi}_{1,N+1}|1,N+1\rangle + \psi_{3,N}|3,N\rangle. \quad (2)$$

Setting the energy of the excited state as zero and with the field phases $\phi_1, \phi_2, \phi_{rf}$ the amplitudes in (2) are

$$\tilde{\psi}_{2,N-1} = e^{-i(\phi_2+\phi_{rf})}\, e^{-i(\omega_{L2}+\omega_{rf})t}\, \psi_{2,N-1}, \quad (3)$$

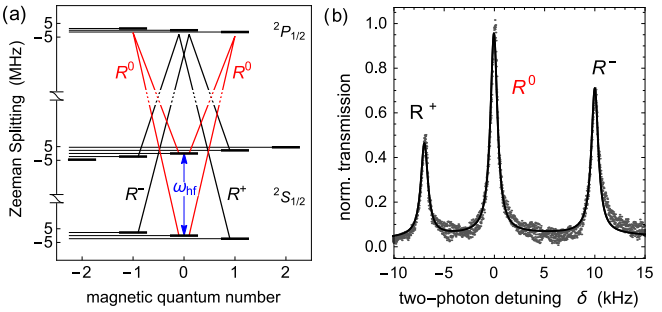

FIG. 1. (Color online) (a) Zeeman splitting of D_1 transition levels of ^{87}Rb. (b) EIT resonances observed at 3.2 G. The transmission is normalized to the R^0 resonance. The full line shows the fit of the gray data points by three Lorentzians [full width at half maximum (FWHM) of 850 ± 50 Hz].

$$\tilde{\psi}_{1,N} = e^{-i\phi_1}\, e^{-i\omega_{L1}t}\, \psi_{1,N}, \tag{4}$$

$$\tilde{\psi}_{2,N} = e^{-i\phi_2}\, e^{-i\omega_{L2}t}\, \psi_{2,N}, \tag{5}$$

$$\tilde{\psi}_{1,N+1} = e^{-i(\phi_1-\phi_{\rm rf})}\, e^{-i(\omega_{L1}-\omega_{\rm rf})t}\, \psi_{1,N+1}. \tag{6}$$

In a second step we dress the lower ground-state pair $(|2N-1\rangle, |1N\rangle)$ with optical photons of laser 1 and the upper ground-state pair $(|2N\rangle, |1N+1\rangle)$ with photons of laser 2. With the detunings $\Delta_1 = \omega_{L1} - (\omega_3 - \omega_1)$ and $\Delta_2 = \omega_{L2} - (\omega_3 - \omega_2)$, assuming equal Rabi frequencies $g_1 = g_2 = g$ for the two optical fields and the rf Rabi frequency $\mathcal{G}$ we obtain for the Hamiltonian

$$\tilde{\mathcal{H}} = \frac{1}{2}\begin{pmatrix} 2(\Delta_1 - \delta_{\rm rf}) & \mathcal{G} & 0 & 0 & 0 \\ \mathcal{G} & 2\Delta_1 & 0 & 0 & g \\ 0 & 0 & 2\Delta_2 & \mathcal{G} & g \\ 0 & 0 & \mathcal{G} & 2(\Delta_2 + \delta_{\rm rf}) & 0 \\ 0 & g & g & 0 & 0 \end{pmatrix}. \tag{7}$$

With this Hamiltonian the quantum master equation

$$\frac{\partial \rho}{\partial t} = -\frac{i}{\hbar}[\tilde{\mathcal{H}}, \rho] + \tilde{\mathcal{L}}_1\rho + \tilde{\mathcal{L}}_2\rho \tag{8}$$

can be solved numerically. We give explicit expressions for the Liouvillian terms $\tilde{\mathcal{L}}$ in the Appendix. Typical steady-state

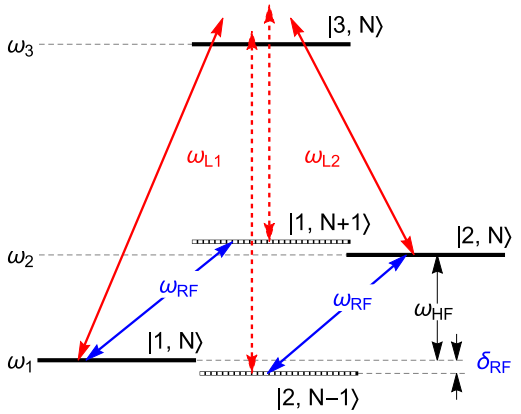

FIG. 2. (Color online) Five-level system of dressed atom ground-state pair and excited state. N signifies the number of rf photons.

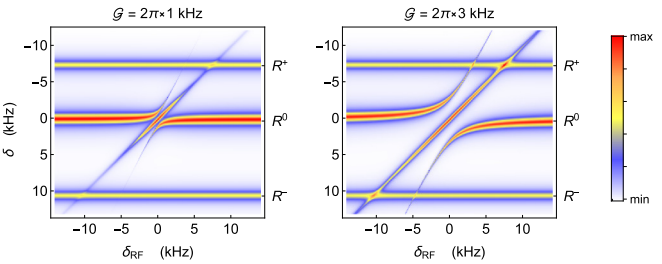

FIG. 3. (Color online) Simulation of transmission as a function of rf detuning $\delta_{\rm rf}$ with $g = 2\pi \times 300$ kHz, $\Gamma = 2\pi \times 190$ MHz, and $\gamma = 2\pi \times 20$ Hz for two rf Rabi frequencies $\mathcal{G}$.

solutions for the optical absorption measure $\mathrm{Im}[\rho_{15} + \rho_{25} + \rho_{35} + \rho_{45}]$ are shown in Fig. 3.

The EIT resonances R^+ and R^- were added to this numerical result; they remain unaffected by the rf field over the detuning range used here. Numerical solutions for the time-dependent master equation (8) are discussed in Sec. V C.

A. Analytical model

A simple model can be derived from diagonalization of (7) in the limit $g \to 0$. The interacting dressed-state eigenvectors which result are explicitly quoted in Fig. 4 along the respective rf Stark shifted energy levels. The letters C and S abbreviate $\cos\beta$ and $\sin\beta$ where the mixing angle β describes the microwave interaction,

$$\beta = \frac{1}{2}\arctan\frac{\mathcal{G}}{\delta_{\rm rf}}. \tag{9}$$

In the limit of weak optical fields these levels participate in two classes of EIT, a linear and a nonlinear resonance. Two linear resonances appear at the two-photon detuning $\delta = \delta_{\rm rf}$, marked by the respective Raman transitions in Fig. 4. They involve the superposition of two pairs of eigenvectors of equal rf photon number N,

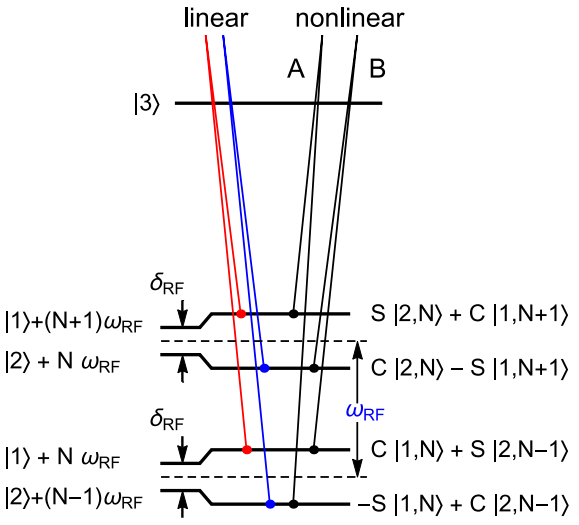

FIG. 4. (Color online) The origin of rf-assisted EIT resonances in the model of interacting dressed states are the coherent Raman transitions between manifolds $\mathcal{E}(N)$ and $\mathcal{E}(N-1)$.

$$\{+\cos\beta\,|1,N\rangle,\ +\sin\beta\,|2,N\rangle\}, \tag{10}$$

$$\{-\sin\beta\,|1,N\rangle,\ +\cos\beta\,|2,N\rangle\}. \tag{11}$$

Equivalent resonances of identical property appear with eigenvectors of other rf photon numbers when using the manifolds $\mathcal{E}(N-1)$, $\mathcal{E}(N+1)$, . . . etc.

The strength of the linear EIT resonance is controlled by the sum of the squared products of the $|1,N\rangle$ and $|2,N\rangle$ amplitudes in (10) and (11), weighted by the respective reduced population Π_i in the bare dressed state,

$$(\sin\beta\cos\beta)^2\,\Pi_1 \quad \text{and} \quad (-\sin\beta\cos\beta)^2\,\Pi_2\,. \tag{12}$$

In our experiment $g \gg \mathcal{G}$ and hence the populations Π_i are controlled by the optical fields. For $g_1 = g_2 = g$ the three-level model [1] predicts for the dark state $\Pi_1 = \Pi_2 = \frac{1}{2}$. With this the sum of contributions (12) to the linear resonance predicts for the optical transmission

$$T_{\rm lin} = \frac{1}{2}\,\sin(2\beta)^2 = \frac{1}{2}\,\frac{\mathcal{G}^2}{\mathcal{G}^2+\delta_{\rm rf}^2}, \tag{13}$$

a Lorentzian distribution around $\delta_{\rm rf} = 0$ which we multiplied by a factor of 2 for reasons of normalization. We see that the spectral width of transmission along the axis of detuning is controlled by the rf intensity.

The two nonlinear EIT resonances in Fig. 4 appear at the two-photon detunings

$$\delta^{\pm} = \delta_{\rm rf} \mp \sqrt{\mathcal{G}^2+\delta_{\rm rf}^2}. \tag{14}$$

They involve opposing levels of neighboring manifolds,

$$\{-\sin\beta|1,N\rangle,+\sin\beta|2,N\rangle\}, \quad (A) \tag{15}$$

$$\{+\cos\beta|1,N\rangle,+\cos\beta|2,N\rangle\}, \quad (B) \tag{16}$$

and they merge with the EIT dip of R^0 at large rf detuning. Their transmission is (again we multiply by a factor of 2 for reasons of normalization)

$$T_{\rm nl}^{(A)} = \sin^4\beta \quad \text{and} \quad T_{\rm nl}^{(B)} = \cos^4\beta\,. \tag{17}$$

The sum $T_{\rm lin} + T_{\rm nl}^{(A)} + T_{\rm nl}^{(B)}$ is 1, independent of detuning and rf intensity, normalized to the intensity of the unperturbed R^0 resonance. In the limit of large positive detuning $\delta_{\rm rf}$, we have $\beta \to 0$ and $T_{\rm nl}^{(B)} \to 1$, the transmission of the unperturbed R^0 resonance. On the other hand, in the limit of large negative detuning $\delta_{\rm rf}$, we have $\beta \to \pi/2$ and $T_{\rm nl}^{(A)} \to 1$. At $\delta_{\rm rf} = \delta = 0$ the transmission at the linear resonance is $T_{\rm lin} = 1/2$, while $T_{\rm nl}^{(A)}$ and $T_{\rm nl}^{(B)}$ are each 1/4. The predictions Eqs. (13) and (17) are in quantitative agreement with the spectra obtained numerically from the master equation in Fig. 3.

III. EXPERIMENT

The experimental setup has been described previously [17]. We use a neon-buffered Rb gas cell containing isotopically pure ^{87}Rb at a neon pressure of 20 Torr kept at 25 °C. The cell is mounted in an rf cavity. Coils in Helmholtz configuration ensure a homogeneous magnetic field along the direction of laser beam propagation. The two lasers are locked via an optical phase lock loop (OPLL) [18]. One of the lasers is kept at the D_1 line of ^{87}Rb using frequency modulation (FM) spectroscopy. The laser beams are merged in an optical fiber and expanded to a diameter of 15 mm before entering the Rb cell. An rf synthesizer (Hittite HMC C070) provides an output power of 20 dBm for driving the ground-state transition. We use fixed attenuators and feed the signal into the resonator by a magnetic coupling loop. Phase stability is guaranteed by referencing the rf generator and the OPLL controls to a GPS-based frequency standard. Phase changes in the rf signal are realized by changing the GPS reference signal line to the synthesizer using a voltage-controlled phaseshifter (MiniCircuits JHPHS-12).

The 40.2-mm-long and 46.8-mm-diameter rf cavity is made of aluminum; it supports the TE_{011} mode near the resonance frequency $\omega_{\rm hf}$. Following the concepts of Godone *et al.* [19], we first estimated the shift due to insertion of the Rb cell using the unperturbed field eigenvectors to derive resonator dimensions. These were refined in CST MICROWAVE STUDIO simulations using actual dimensions, including laser ports, coupling loop, and the empty Rb cell to match the pressure-shifted hyperfine splitting [20]. The Rb glass cell has a long glass stem which ensures condensation of the Rb outside the cavity, thus minimizing the rf-sensitive load. The cell interior length and diameter are 22 and 21 mm, respectively. The length is chosen to be one-half of the wavelength corresponding to the hyperfine frequency. Fine tuning of the cavity is accomplished by length adjustment using a low-pitch screwable lid.

Figure 5 shows the inhomogeneity of the magnetic amplitude component $|H_z|$ over the cross section of the cell. The loaded Q factor of the resonator is measured to be 1350 at $\omega = \omega_{\rm hf}$ with a full width at half maximum of 5 MHz; see the reflected power at resonance in Fig. 5.

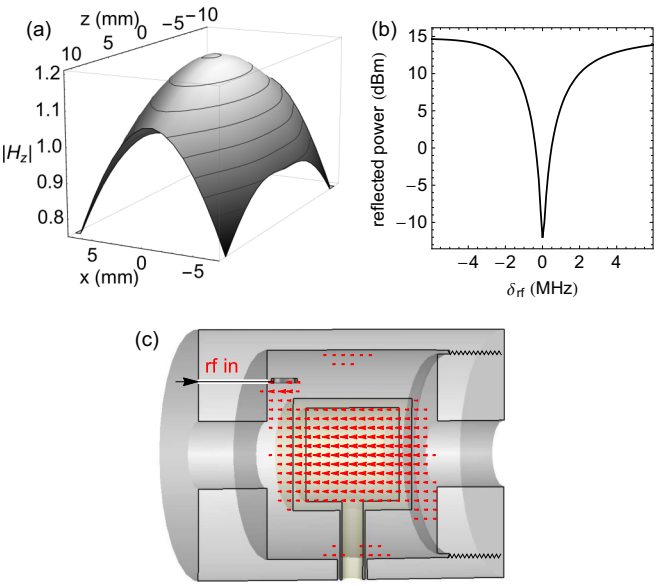

FIG. 5. (Color online) (a) z component of magnetic field amplitude in the observation volume, normalized to the mean value; the contours mark 5% levels. (b) measured reflected power as a function of rf detuning from 6.8569 GHz. (c) Three-dimensional (3D) view of cavity and cell. Magnetic field vectors with magnitude greater than 30% of the peak value are shown in the plane of cut.

IV. RESULTS

Sample scans of EIT spectra are presented in Fig. 6 as a function of rf detuning for different rf powers.

The linear dependence $\delta = \delta_{\rm rf}$ for the linear resonance is apparent from the figures. We find quantitative agreement of the transmitted optical intensity along the diagonal $\delta = \delta_{\rm rf}$ with the simple model (13).

Figure 7, right, shows the optical transmission at the linear resonance, relative to the transparency of the R^0 resonance at large detuning. The full lines represent fits of Eq. (13). They provide absolute values for the mean rf Rabi frequencies in the observation volume. We obtain $\mathcal{G}_{\rm expt} = 2.8 \pm 0.2, 9 \pm 0.5$, and 25 ± 5 kHz for the powers -20, -10, and 0 dBm, respectively. This is in agreement with the expected square-root scaling with rf power,

$$\mathcal{G} = \Delta g\, \mu_B |B_z|/\hbar, \tag{18}$$

where μ_B is Bohr's magneton and $\Delta g = (g_{F=2} - g_{F=1})$ is the difference in g factors of the ground hyperfine states $F = 2$ and $F = 1$ and in agreement with the anticipated separation of

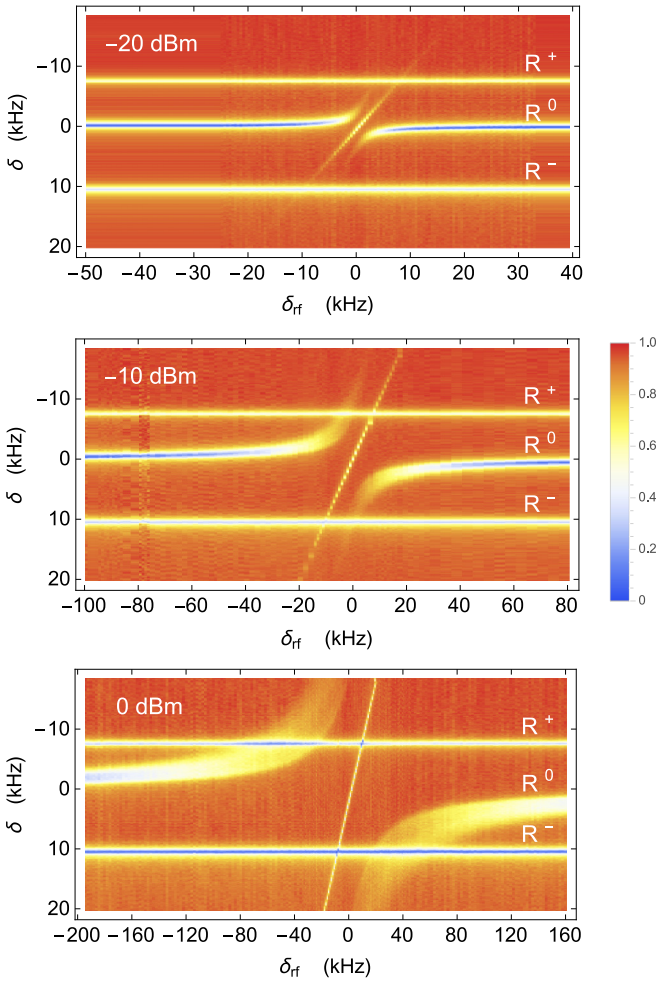

FIG. 6. (Color online) Experimental two-photon absorption spectra recorded at cavity power imputs of -20, -10, and 0 dBm. The color scale ranges from normal (1) to minimal absorption (0) in each figure. The respective mean magnetic Rabi frequencies are measured to be $\mathcal{G}/2\pi \approx 3$, 9, and 25 kHz; see Fig. 7(b).

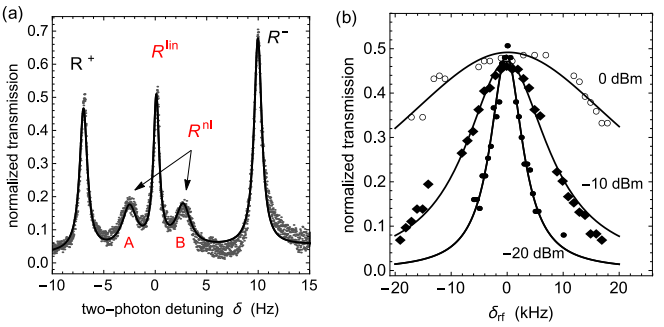

FIG. 7. (Color online) (a) resonance tripling of R^0 at $\delta_{\rm rf} = 0$, recorded at -20 dBm. The width of the linear resonance is 630 ± 50 Hz, of the nonlinear resonance ≈ 2 kHz. (b) Transmission at linear resonance along the diagonal $\delta = \delta_{\rm rf}$, relative to that of R^0 at large detuning. Full curves represent fit of Eq. (13).

resonances A and B, $2\mathcal{G}$ at $\delta_{\rm rf} = 0$. Maximizing the frequency separation between these resonances serves as a precise indicator in fine-tuning the cavity. The measured transmission at $\delta_{\rm rf} = 0$ demonstrates the agreement between experiment and the prediction of the simple model for the resonance intensities; see Fig. 7(b). Equations (13) and (17) predict $T_{\rm nl}^{(A)} : T_{\rm lin} : T_{\rm nl}^{(B)} = \frac{1}{4} : \frac{1}{2} : \frac{1}{4}$ relative to that at the R^0 resonance position at large detuning. The observed nonlinear peaks are somewhat lower, $\frac{1}{5} : \frac{1}{2} : \frac{1}{5}$, a consequence of inhomogeneous broadening; see Sec. V B.

The color (gray-scale) coding in Fig. 6 serves to emphasize the additivity of transparency. At low rf power the R^0 resonance shows the highest transparency. At higher powers this transparency splits over the linear and two nonlinear resonances, and we notice enhanced transparency when linear and nonlinear resonances cross the R^+ and R^- positions in the 0 dBm measurement. This additivity is a consequence of the fact that R^+, R^0, and R^- involve independent ground-state Zeeman levels.

General agreement is obtained in comparison with the simulations shown in Fig. 3 *with exception* for the width of the nonlinear resonances near $|\delta_{\rm rf}| = 0$. They are much wider in the experiment. We attribute this to the inhomogeneity of the rf amplitude in the observation volume. This feature and the observed response of the resonances to sudden frequency or phase switching will be treated in the Discussion.

V. DISCUSSION

A. Mollow-type triplet

The observed tripling of an EIT resonance in the presence of a near-resonant rf field is reminescent of the Mollow triplet [16]. The role taken by the spontaneous emission rate Γ in the Mollow triplet is here taken by the generalized scattering rate of optical photons by the EIT ground-state levels [20],

$$\Gamma' = g^2/\Gamma + \gamma. \tag{19}$$

Here we assumed equal optical Rabi frequencies $g_1 = g_2 = g$, while γ is the ground-state dephasing rate due to collisions and diffusive loss from the observation volume. The coherent two-photon connection between the ground states $|1\rangle$ and $|2\rangle$ as indicated by the optical Raman transitions in Fig. 4 is

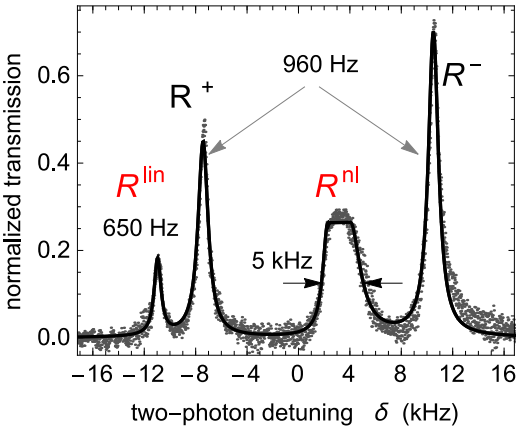

FIG. 8. (Color online) Resonance tripling of R^0 at $\delta_{\rm rf} = 11$ kHz, recorded at -10 dBm. The width of the linear resonance is 650 ± 50 Hz, and of the nonlinear resonance B is $\approx$5 kHz. Resonance A is exceedingly weak and outside the scan widow. Data points represent experimental results, the full line a fit of Lorentzians.

interrupted at the rate (19) and thus is the origin for broadening of the EIT resonance, the quantity $2\Gamma'$ being a measure for the FWHM of the R^0 resonance [20]. Γ' should also be influential for the rf-induced resonances. We were unable to deduce analytical expressions for their widths but we note that the observations and the numerical predictions reveal substantial narrowing of the linear resonance see Fig. 7 at resonance, but also, for detuned rf fields, see Fig. 8.

The numerical simulations predict even narrower widths for the nonlinear resonance A when $\delta_{\rm rf} > 0$ and for resonance B when $\delta_{\rm rf} < 0$; see Fig. 3. The experimental widths for nonlinear resonances are however substantially wider, a consequence of the inhomogeneity of the microwave field, which we discuss next.

B. Inhomogeneity of the rf field

To demonstrate the effect of rf-field inhomogeneity we consider the field profile in the observation volume (Fig. 5) and evaluate at a fixed value of $\delta_{\rm rf}$ the contributions of the three rf-induced resonances separately for each volume element and sum the contributions. Such a simulation is shown for $\mathcal{G}/2\pi = 25$ kHz and a homogeneous 12-mm-diameter laser beam in Fig. 9.

The linear resonance is narrow as its spectral position is independent of the rf power; however the widths of the nonlinear resonances broaden substantially, similarly to what is observed in our experiment. This broadening represents an inhomogeneous width.

The homogeneous width of an EIT resonance is controlled by the scattering rate Γ' in Eq. (19). The quantities g and Γ are identical for the linear and nonlinear resonances. The diffusive loss rate of atoms from the observation volume is included in γ and this rate is different for linear and nonlinear resonances due to the effective size of the volume: For the linear resonance the cylindrical observation volume is given by the size of the laser beams. This large volume yields $\gamma \approx 2\pi \times 20$ Hz.

On the other hand the effective volume for the nonlinear resonance is defined by lengths beyond which the frequency

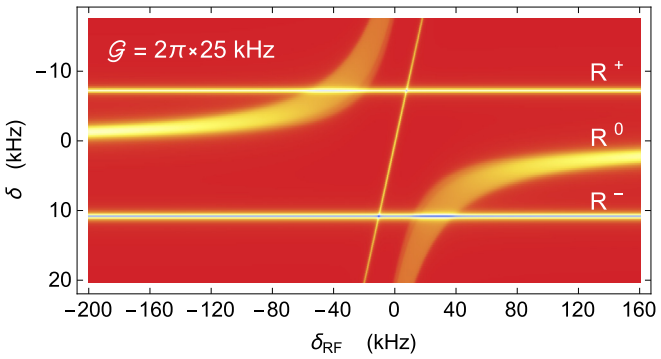

FIG. 9. (Color online) Simulation of 0 dBm spectrum of Fig. 6, accounting for the magnetic field inhomogeneity in the observation volume. The EIT resonances R^+ and R^- were added to this simulation; they remain unaffected by the rf field.

position of the resonance changes by the homogeneous width of a stationary atom. To estimate this volume we consider a distance measure for diffusive loss over which the resonance position shifts by $\Gamma' \approx 2\pi \times 1$ kHz. The CST simulations in Fig. 5 show that the magnetic field amplitude changes by this amount over distances $d \approx 2$ mm. Since γ scales with d^{-2} [see Eq. (43) of [20]] we estimate that the diffusive contribution to $\gamma/2\pi$ for the nonlinear resonance is in the kilohertz range. The enhanced diffusive loss from the small effective observation volume explains the anomalous widths of the nonlinear resonances in the experimental results in Figs. 7 and 8.

C. Response to optical frequency and phase jumps

The difference in rates Γ' for the linear and nonlinear resonances is also observable in the rate at which the optical transparency of the EIT medium responds to departures from a resonantly balanced electromagnetic field term $e^{i(\omega_{\rm hf}t+kz-\phi)}$

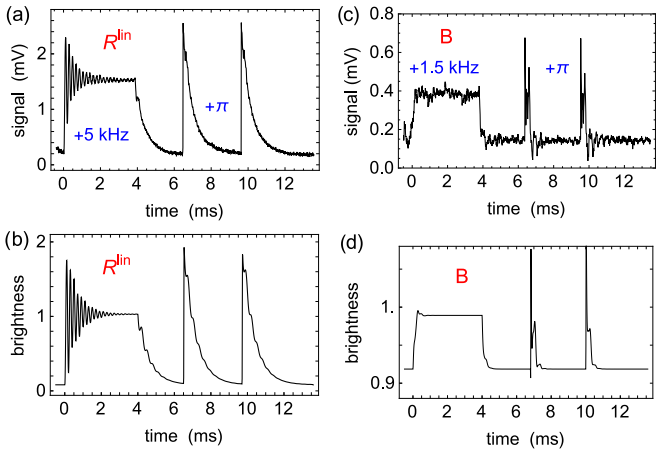

FIG. 10. (Color online) Photodiode signal showing the increase in absorption following a frequency jump away from resonance at $t = 0$, (a) for the linear resonance and (c) for resonance B. Returning to resonance (at $t = 4$ μs) EIT conditions are reached again in an exponential fashion. This is also observed after a sudden jump of the optical phase difference by π (time period between 6.5 and 9.5 ms). The bottom row gives the expected absorption strength in units of brightness from numerical solution of (9) using the parameters in Table I.

TABLE I. Parameters used in numerical simulation (multiply all rates by 2π, $\Gamma = 190$ MHz, $\mathcal{G} = 3.3$ kHz, $g = 300$ kHz).

	$\delta_{\rm rf}$ (kHz)	γ (Hz)	$\Delta\delta$ (kHz)	$\Delta\phi_{\rm opt}$ (kHz)	$\Delta\phi_{\rm rf}$	Resonance
Fig. 10(b)	0	20	+ 5.0	π		$R^{\rm lin}$
Fig. 10(d)	0	1000	+ 1.5	π		$R^{\rm nl}$ B
Fig. 11(b)	0, 3, 6	20			0.8π	$R^{\rm lin}$
Fig. 12(a)	0, 3, 6	20			Variable	$R^{\rm lin}$
Fig. 12(b)	1	1000			Variable	$R^{\rm nl}$ B
Fig. 13(b)	1	1000			$\pi/2$	$R^{\rm nl}$ B
Fig. 13(b)	3,10	200			$\pi/2$	$R^{\rm nl}$ B

in (1). A sudden change in two-photon detuning by $\Delta\delta$ leads to temporal departure from the time-dependent coherent superposition (1), manifested by Rabi oscillations at frequency $\Delta\delta$. The oscillations are damped at the rate Γ', upon which the medium resorts to regular incoherent absorption.

The reverse process, sudden switching of the two-photon detuning to zero, establishes the path to commensurate oscillations of the optical difference field and the state amplitudes at the frequency $\omega_{\rm hf}$ in (1). EIT is then approached in exponential fashion with time constant $\tau \propto 1/\Gamma'$, because Γ' signifies the effective scattering rate at which a decision to populate the dark-state superposition (1) can occur [17]. This exponential decay into EIT conditions is also observed following a sudden change in the optical phase ϕ in (1).

As example we consider $R^{\rm lin}$, prepared at $t < 0$ at resonance $\delta = \delta_{\rm rf} = 0$; see Figs. 10(a) and 10(b). To increase the spectral separation between resonances we use here and in the following a slightly higher magnetic field (4.8 G).

At $t = 0$ ms the two-photon detuning is switched from zero to $\delta = 5$ kHz and back to zero again at $t = 4$ ms. The slow decay upon exiting EIT and the slow recovery when returning to resonance are consistent with the small value of γ, as also shown by the simulation. The simulation interprets this phase response by the measure *brightness*, defined as the response relative to that of a dark state to an optical phase shift of $\pm\pi/2$; see [17,21]. Likewise the response to an optical phase jump by π observed is reproduced by the simulation using a small value of γ. Parameters used in the simulations are collected in Table I.

The response is very different for the nonlinear resonance; see Figs. 10(c) and 10(d). Here we exit from resonance B by a 1.5 kHz frequency jump at $t = 0$ and return to resonance at $t = 4$ ms. The nonlinear resonance responds rapidly to changes in frequency or phase, consistent with the higher rate γ.

D. Response to rf phase jumps

The response to sudden phase shifts of the rf field is different from that for the optical field. At $R^{\rm lin}$ the optical and rf detunings are equal, a condition straightforward to adjust in the experiment at any detuning. In Fig. 11 we compare examples of experimental scans at three values of the rf detuning with simulations.

Here the phase of the rf signal is shifted by $3\pi/4$ at 0.2 ms. Short-duration (30 μs) optical phase shifts of $\pm\pi/2,\pi$ occur at 4.2, 5, and 5.8 ms respectively and serve as a reference for the response in absorption. Following the rf phase shift a momentary increase in absorption is observed, which decays back to EIT conditions at a rate commensurate with the small value of γ. This exponential return to EIT is modulated by oscillations, their frequency increasing with increased detuning. Inspection of the experiment and the simulations reveals that the oscillation occurs at the generalized rf Rabi frequency,

$$\Omega = \sqrt{\mathcal{G}^2 + \delta_{\rm rf}^2}\,. \tag{20}$$

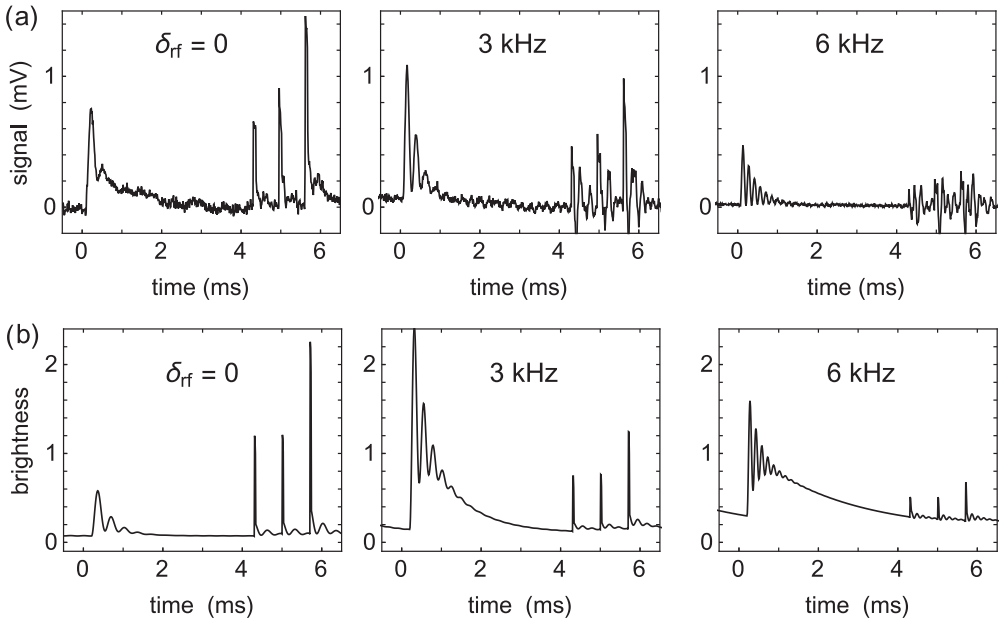

FIG. 11. Effect of rf phase jump at $R^{\rm lin}$ at three values of rf detuning. The phase of the rf signal is shifted by $3\pi/4$ at 0.2 ms. Short-duration (30 μs) optical phase shifts by $\pm\pi/2,\pi$ at the end serve as reference. (a) Photodiode signal, and (b) simulation of the absorption signal in units of brightness using the parameters in Table I.

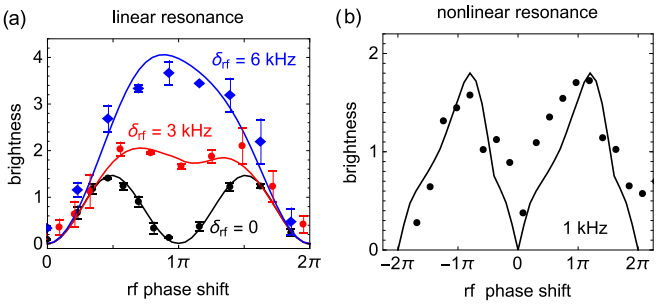

FIG. 12. (Color online) Examples of rf phase-jump-induced absorption, (a) for the linear and (b) for the nonlinear resonance, are shown as points. Simulation results (full lines) are scaled by a factor of 0.85 in (a) and of 6 in (b).

Figure 12 compares observations and simulations of the dependence on the magnitude of the rf phase jump $\Delta\phi_{rf}$.

Most striking is the periodicity by π for $\delta_{rf} = 0$ and its continuous change to a periodicity of 2π as the detuning increases. Parallel to this, the amplitude of absorption following an optical phase jump decreases in comparison to the amplitude following an rf phase jump (see Fig. 11), opposite to what we observe for the nonlinear resonance, which we discuss next.

Figure 13 gives examples for the response to rf phase jumps by $\pi/2$ at the nonlinear resonance B. There is general agreement between the observed brightness and the simulated response; see Fig. 12(b). It is worthwhile to examine the response to the optical phase shifts by $\pm\pi/2$ and π at 4.8, 5.5, and 6.2 ms in Fig. 13. At low rf detuning the response is oscillatory, just as we saw it in Fig. 10 for resonance B at $\delta_{rf} = 0$, but at larger rf detunings this response decays in an exponential fashion, indicating the transition to the unperturbed R^0 resonance which must be described by the lower value of γ.

By the same token the brightness response to a jump in the rf phase diminishes at larger rf detuning, again indicative of the transition to the unperturbed R^0 resonance which is insensitive to the rf field.

E. Simple models for rf phase sensitivity

While practically all observations are correctly reproduced in simulations using the five-level master equation (see Figs. 10–13), it is enlightening to find simple models for the rf phase response. For this purpose we define the R^0 dark state at a fixed position z, in the absence of an rf field,

$$|\psi_D(t)\rangle = \frac{1}{\sqrt{2}}(|1\rangle - e^{i(\omega_{hf}t-\phi)}|2\rangle). \tag{21}$$

The nonlinear resonance A in Fig. 6 develops into the form (21) as $\delta_{rf} \to +\infty$, where the mixing angle is $\beta = 0$. Hence we require that the superposition (15) is, apart from an overall phase,

$$\left|\psi_D^{(A)}(t)\right\rangle = \cos\beta\,(|1,N\rangle + e^{i[\omega_{hf}t-\phi_{rf}(\delta_{rf})-\phi]}\,|2,N\rangle), \tag{22}$$

and we demand for resonance A that $\phi_{rf}(+\infty) = \pm\pi$. On the other hand, we require that the superposition (16)

$$\left|\psi_D^{(B)}(t)\right\rangle = -\sin\beta(|1,N\rangle - e^{i[\omega_{hf}t-\phi_{rf}(\delta_{rf})-\phi]}\,|2,N\rangle) \tag{23}$$

develops into (21) at $\delta_{rf} \to -\infty$; hence resonance B has $\phi_{rf}(-\infty) = 0$. It is interesting that $\phi_{rf}(\delta_{rf})$ changes by π when moving from resonance A to resonance B. We attribute this to the presence of the linear resonance which is embedded in the continuous variable δ_{rf} of the R^0 quantum system.

For the linear resonance the role of the rf phase is more intricate as the mixing angle changes with detuning and leads to imbalance of amplitudes between states $|1\rangle$ and $|2\rangle$ in (10)

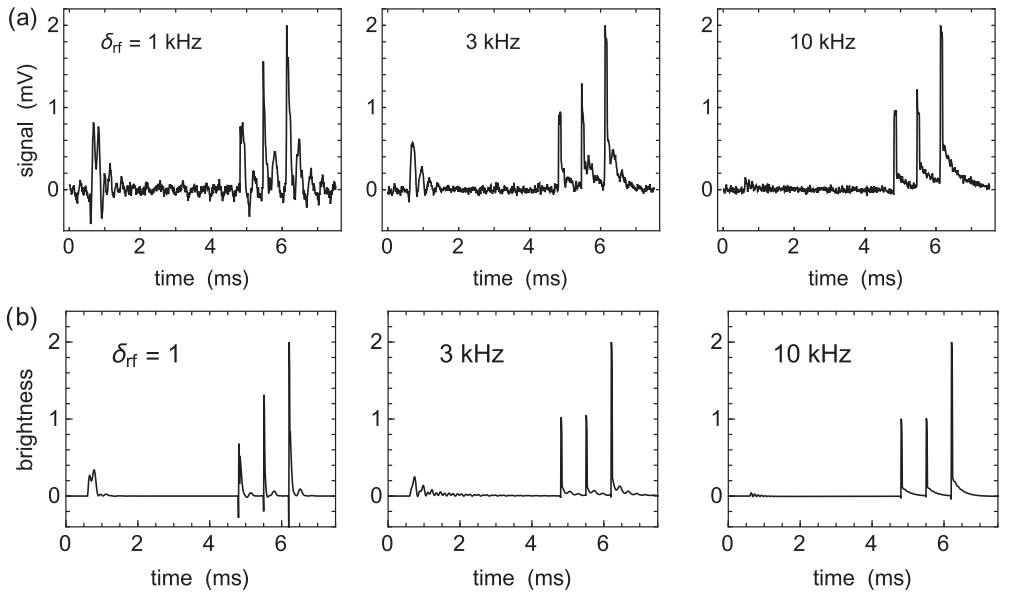

FIG. 13. The photodiode signals following an rf phase jump by $\pi/2$ at the nonlinear resonance B at three detunings are shown in (a). Short-duration (30 μs) optical phase shifts by $\pm\pi/2,\pi$ at the end of the scan serve as reference. (b) Simulation of the absorption signal using the parameters in Table I.

and (11). For $\delta_{\rm rf} = 0$ the analysis is straightforward; we expect for superposition (10)

$$\left|\psi_{\rm lin}^{(1)}(t)\right\rangle = \frac{1}{\sqrt{2}}\left(|1,N\rangle + e^{i[\omega_{\rm hf}t-\phi_{\rm rf}(0)-\phi]}\,|2,N\rangle\right), \tag{24}$$

a dark state when $\phi_{\rm rf}(0) = \pm\pi$. On the other hand for the superposition (11) we expect a dark state

$$\left|\psi_{\rm lin}^{(2)}(t)\right\rangle = -\frac{1}{\sqrt{2}}\left(|1,N\rangle - e^{i[\omega_{\rm hf}t-\phi_{\rm rf}(0)-\phi]}\,|2,N\rangle\right), \tag{25}$$

which requires $\phi_{\rm rf}(0) = 0$ in order to match (21). So it appears that at rf resonance two classes of linear dark states are present, half with rf phase of π and half with phase of 0. This doubling of the linear resonance is in line with the expected intensities and phases of the two nonlinear resonances in the limit of small G near $\delta_{\rm rf} = 0$, when they should merge with the linear resonance. The presence of two solutions for the rf phase for the linear resonance is also borne out in the model of Luo *et al.* [12].

The above predictions from the simple analytical model are in full agreement with rf phase-switching phenomena observed in the experiment. Specific observations at rf resonance $\delta_{\rm rf} = 0$ are that (1) no change in absorption occurs after a phase jump by π at the linear resonance (see Fig. 12), (2) a phase jump by π at either nonlinear resonance A or B leads to a jump in brightness to 2 (experimental data not shown), and (3) a frequency jump from the nonlinear resonance A to B or vice versa leads to a jump in brightness to a level 2 (experimental data not shown).

Predictions for $\delta_{\rm rf} \neq 0$ are more cumbersome and not pursued here. However, it is obvious that for large rf detuning the sensitivity of the nonlinear resonance to the rf phase must diminish. This is a consequence of the transition of the nonlinear to the rf-insensitive R^0 resonance. On the other hand, we observe in both experiment and numerical simulation a loss of sensitivity of the linear resonance to the optical phase when $\delta_{\rm rf} \neq 0$. We found no simple explanation for this behavior—as we also have not been able to formulate a simple model for the relationship between optical and rf phases.

VI. CONCLUSION

We show that near-resonant interaction of an rf field with the ground states of a dark resonance leads to a resonance tripling, reminiscent of an avoided crossing of a quantum continuum with a discrete interloper state [22]. The nonlinear resonances reported here display an avoided crossing in the continuous variable of the rf detuning. The crossing is accompanied by the characteristic phase jump by π and the interloper is the linear resonance which is characterized by sub-EIT linewidth.

The appearance of the nonlinear resonances is of technical interest in that balancing their appearance allows precise adjustment of an rf cavity to resonance condition, e.g. for use as vapor-cell frequency standard [23].

Complex phase relationships between rf and optical fields appear for the three resonances. The experimental observations are confirmed by simulations using a five-level master equation. At selected conditions the phase relationships can be derived using the simple analytical model. A general analytical relationship, however, remains elusive at this point. The many instances in which rf-controlled EIT is envisioned in quantum optics applications warrants further consideration of this topic.

ACKNOWLEDGMENTS

We wish to thank Professor H-P. Breuer for fruitful discussions. We greatly appreciate technical guidance, which was decisive for the construction of the rf cavity, by Dr. Salvatore Micalizio and Dr. Filippo Levi from Istituto Nazionale di Ricerca Metrologica, Torino, Italy. This research was supported by the Deutsche Forschungsgemeinschaft under Grant No. He2525/7-1.

APPENDIX: LIOUVILLIAN

We label the density matrix elements by the numbers 1–5 corresponding to the state labels $|2,N-1\rangle, |1,N\rangle, |2,N\rangle, |1,N+1\rangle, |3,N\rangle$. Following [24] we consider two terms for the Liouvillian. One accounts for spontaneous emission of the excited state $|3N\rangle$ at the rate Γ,

$$\tilde{\mathcal{L}}_1\rho = \frac{\Gamma}{2}\begin{pmatrix} 0 & 0 & 0 & 0 & -\rho_{1,5} \\ 0 & \rho_{5,5} & 0 & 0 & -\rho_{2,5} \\ 0 & 0 & \rho_{5,5} & 0 & -\rho_{3,5} \\ 0 & 0 & 0 & 0 & -\rho_{4,5} \\ -\rho_{5,1} & -\rho_{5,2} & -\rho_{5,3} & -\rho_{5,4} & -2\rho_{5,5} \end{pmatrix}, \tag{A1}$$

and there is a second term for dephasing and hyperfine-changing collisions in the ground states at the rate γ,

$$\tilde{\mathcal{L}}_2\rho = -\frac{\gamma}{2}\begin{pmatrix} 2(\rho_{11}-\rho_{44}) & 2\rho_{12} & 2\rho_{13} & 2\rho_{14} & \rho_{15} \\ 2\rho_{21} & 2(\rho_{22}-\rho_{33}) & 2\rho_{23} & 2\rho_{24} & \rho_{25} \\ 2\rho_{31} & 2\rho_{32} & 2(\rho_{33}-\rho_{22}) & 2\rho_{34} & \rho_{35} \\ 2\rho_{41} & 2\rho_{42} & 2\rho_{43} & 2(\rho_{44}-\rho_{11}) & \rho_{45} \\ \rho_{51} & \rho_{52} & \rho_{53} & \rho_{54} & 0 \end{pmatrix}. \tag{A2}$$

[1] M. Orszag, *Quantum Optics* (Springer, Berlin, 2000).
[2] Y.-x Liu, J. Q. You, L. F. Wei, C. P. Sun, and F. Nori, Phys. Rev. Lett. **95**, 087001 (2005).
[3] H. Ian, Y.-x Liu, and F. Nori, Phys. Rev. A **81**, 063823 (2010).
[4] P. C. de Groot, J. Lisenfeld, R. N. Schouten, S. Ashhab, A. Lupascu, C. J. P. M. Harmans and J. E. Mooij, Nat. Phys. **6**, 763 (2010).
[5] J. Q. You and F. Nori, Nature (London) **474**, 589 (2011).

[6] F. Deppe, M. Mariantoni, E. P. Menzel, A. Marx, S. Saito, K. Kakuyanagi, H. Tanaka, T. Meno, K. Semba, H. Takayanagi, E. Solano, and R. Gross, Nat. Phys. **4**, 686 (2008).
[7] A. Eilam, A. D. Wilson-Gordon, and H. Friedmann, Opt. Lett. **34**, 1834 (2009).
[8] Z. H. Xiao, S. G. Shin, and K. Kim, J. Phys. B **43**, 161004 (2010).
[9] R. Sadighi-Bonabi and T. Naseri, Appl. Opt. **54**, 3484 (2015).
[10] J. O. Weatherall and C. P. Search, Phys. Rev. A **78**, 053802 (2008).
[11] R. Yu, J. Li, P. Huang, A. Zheng, and X. Yang, Phys. Lett. A **373**, 2992 (2009).
[12] B. Luo, H. Tang, and H. Guo, J. Phys. B **42**, 235505 (2009).
[13] M. S. Shahriar and P. R. Hemmer, Phys. Rev. Lett. **65**, 1865 (1990).
[14] H. Li, V. A. Sautenkov, Y. V. Rostovtsev, G. R. Welch, P. R. Hemmer, and M. O. Scully, Phys. Rev. A **80**, 023820 (2009).
[15] E. A. Wilson, N. B. Manson, C. Wei, and L. Yang, Phys. Rev. A **72**, 063813 (2005).
[16] C. Cohen-Tannoudji, J. Dupont-Roc, and G. Grynberg, *Atom-Photon Interactions* (Wiley, New York, 1992), pp. 427–443.
[17] C. Basler, K. Reininger, F. Meinert, P. N. Ghosh, and H. Helm, Phys. Rev. A **87**, 013430 (2013).
[18] J. Appel, A. MacRae, and A. I. Lvovsky, Meas. Sci. Technol. **20**, 055302 (2009).
[19] A. Godone, S. Micalizio, F. Levi, and C. Calosso, Rev. Sci. Instrum. **82**, 074703 (2011).
[20] F. Meinert, C. Basler, A. Lambrecht, S. Welte, and H. Helm, Phys. Rev. A **85**, 013820 (2012).
[21] T. Abi-Salloum, J. P. Davis, C. Lehman, E. Elliott, and F. A. Narducci, J. Mod. Opt. **54**, 2459 (2007).
[22] M. Aymar, C. H. Greene, and E. Luc-Koenig, Rev. Mod. Phys. **68**, 1015 (1996).
[23] A. Godone, F. Levi, and S. Micalizio, Phys. Rev. A **65**, 033802 (2002).
[24] M. Roghani, H.-P. Breuer, and H. Helm, Phys. Rev. A **81**, 033418 (2010).